

Magnetic diagnostics layout design for CFETR plasma equilibrium reconstruction

Qingze Yu(于庆泽), Yao Huang(黄耀), Zhengping Luo(罗正平), Yuehang Wang(汪悦航), Zijie Liu(刘自结), Wangyi Rui(芮望颐), Kai Wu(吴凯), Bingjia Xiao(肖炳甲), and Jiangang Li(李建刚)

Citation: Chin. Phys. B, 2024, 33 (**4**): 045201. DOI: 10.1088/1674-1056/ad23d6
Journal homepage: http://cpb.iphy.ac.cn; http://iopscience.iop.org/cpb

What follows is a list of articles you may be interested in

Theoretical analyses on the one-dimensional charged particle transport in a decaying plasma under an electrostatic field

Yao-Ting Wang(汪耀庭), Xin-Li Sun(孙鑫礼), Lan-Yue Luo(罗岚月), Zi-Ming Zhang(张子明), He-Ping Li(李和平), Dong-Jun Jiang(姜东君), and Ming-Sheng Zhou(周明胜)
Chin. Phys. B, 2023, 32 (**9**): 095201. DOI: 10.1088/1674-1056/ace033

Upgrade of the magnetic diagnostic system for restart of HT-6M operation

Li-Xing Chen(陈力行), Biao Shen(沈飙), Da-Long Chen(陈大龙), Zheng-Ping Luo(罗正平),Zu-Chao Zhang(张祖超), Ying Chen(陈颖), Yong Wang(王勇), and Jin-Ping Qian(钱金平)
Chin. Phys. B, 2022, 31 (**12**): 125203. DOI: 10.1088/1674-1056/ac7f93

Numerical simulation of anode heat transfer of nitrogen arc utilizing two-temperature chemical non-equilibrium model

Chong Niu(牛冲), Surong Sun(孙素蓉), Jianghong Sun(孙江宏), and Haixing Wang(王海兴)
Chin. Phys. B, 2021, 30 (**9**): 095206. DOI: 10.1088/1674-1056/ac133a

Plasma shape optimization for EAST tokamak using orthogonal method

Yuan-Yang Chen(陈远洋), Xiao-Hua Bao(鲍晓华), Peng Fu(傅鹏), Ge Gao(高格)
Chin. Phys. B, 2019, 28 (**1**): 015201. DOI: 10.1088/1674-1056/28/1/015201

Fast parallel Grad-Shafranov solver for real-time equilibrium reconstruction in EAST tokamak using graphic processing unit

Yao Huang(黄耀), Bing-Jia Xiao(肖炳甲), Zheng-Ping Luo(罗正平)
Chin. Phys. B, 2017, 26 (**8**): 085204. DOI: 10.1088/1674-1056/26/8/085204

Magnetic diagnostics layout design for CFETR plasma equilibrium reconstruction

Qingze Yu(于庆泽)[1,2], Yao Huang(黄耀)[1,†], Zhengping Luo(罗正平)[1], Yuehang Wang(汪悦航)[1], Zijie Liu(刘自结)[3], Wangyi Rui(芮望颐)[1,2], Kai Wu(吴凯)[1], Bingjia Xiao(肖炳甲)[1,2], and Jiangang Li(李建刚)[1,2]

[1] *Institute of Plasma Physics, Hefei Institute of Physical Science, Chinese Academy of Sciences, Hefei* 230031, *China*
[2] *University of Science and Technology of China, Hefei* 230026, *China*
[3] *College of Physics and Optoelectronic Engineering, Shenzhen University, Shenzhen* 518060, *China*

(Received 23 November 2023; revised manuscript received 18 January 2024; accepted manuscript online 30 January 2024)

Plasma equilibrium reconstruction provides essential information for tokamak operation and physical analysis. An extensive and reliable set of magnetic diagnostics is required to obtain accurate plasma equilibrium. This study designs and optimizes the magnetic diagnostics layout for the reconstruction of the equilibrium of the plasma according to the scientific objectives, engineering design parameters, and limitations of the Chinese Fusion Engineering Test Reactor (CFETR). Based on the CFETR discharge simulation, magnetic measurement data are employed to reconstruct consistent plasma equilibrium parameters, and magnetic diagnostics' number and position are optimized by truncated Singular value decomposition, verifying the redundancy reliability of the magnetic diagnostics layout design. This provides a design solution for the layout of the magnetic diagnostics system required to control the plasma equilibrium of CFETR, and the developed design and optimization method can provide effective support to design magnetic diagnostics systems for future magnetic confinement fusion devices.

Keywords: plasma equilibrium reconstruction, EFIT code, flux loops and magnetic probes, optimization

PACS: 52.55.Fa, 28.52.–s, 52.70.Ds, 52.55.–s **DOI:** 10.1088/1674-1056/ad23d6

1. Introduction

Chinese Fusion Engineering Testing Reactor (CFETR) is a novel generation of fusion energy utilization reactors in China, aiming to bridge the gap between ITER and DEMO. Based on the current tokamak research and the basis of ITER, the primary goal of the first phase is to achieve steady-state operation and tritium self-sustaining, with a modest fusion power of up to 200 MW. Phase II mainly aims to validate DEMO with a fusion power over 1 GW.[1,2] Magnetic fields are up to 6.5 T, a specified plasma shape with an elongation of 2, the plasma current is 14 MA, and the major and minor radii are 7.2 m and 2.2 m, respectively.

The plasma shape and other parameters, such as $\beta_{\rm p}$ and $l_{\rm i}$ are critical for the tokamak device operation. One of the basic problems of the tokamak operation is the establishment of a plasma equilibrium configuration that can stably confine the high-temperature plasma. Fitting external magnetic measurement information based on equilibrium reconstruction such as the EFIT[3,4] code effectively obtains plasma discharge configurations. The magnetic measurements required by reconstruction algorithms generally involve flux loops and magnetic probes that measure the magnetic flux and magnetic field locally.[5]

At present, the magnetic diagnostics design schemes for plasma equilibrium control in the world's major tokamak devices are very mature, such as JET,[6] KSTAR,[7] DIIID,[8] and EAST.[9] However, design schemes for large devices such as fusion reactors have not yet been applied in experiments. Currently, only ITER has a relatively mature design and some exploration of DEMO.[10,11] As the next-generation fusion reactor of ITER, CFETR has a more complex structure and a harsh nuclear environment, making it impossible to replicate existing solutions directly.

At present, the most common design methods are dense distribution, and optimization through truncated singular value decomposition (TSVD),[12,13] Fourier analysis,[14] integer linear programming,[15] and data validity and sensitivity analysis.[16] In addition, the material and processing technology for magnetic diagnostics can be optimized to make the plasma equilibrium reconstruction more accurate.[17,18]

This study designs and optimizes the magnetic diagnostics layout for the reconstruction of the equilibrium of the plasma according to the scientific objectives, engineering design parameters, and limitations of the CFETR. According to the CFETR discharge simulation,[19] the magnetic measurement data of the complete discharge was simulated by EFIT code, and the consistent plasma equilibrium was reconstructed accordingly, which verified the effectiveness of the magnetic diagnostics layout design. On this basis, the TSVD method is used to optimize the number and location of magnetic diag-

†Corresponding author. E-mail: yaohuang@ipp.ac.cn

© 2024 Chinese Physical Society and IOP Publishing Ltd

nostics, and the redundancy reliability of the design is verified.

The structure of the current paper is as follows: Section 2 describes the preliminary design of CFETR magnetic diagnostics. Section 3 illustrates the optimization approach. The results attained using the EFIT code are given in Section 4. Section 5 concludes the paper.

2. Prellminary design of CFETR magnetic diagnostics

The preliminary dense distribution design of the flux loops and magnetic probes of CFETR is performed. As is well known, flux loops cannot be arranged in positions with windows; although the closer the magnetic probe is to the plasma, the more advantageous it is for reconstruction, the radiation inside the blanket is severe and installation is difficult. Given the engineering limitations, the flux loops are densely distributed in the position without windows on the vacuum chamber wall, 117 in total, as shown in Fig. 1(a). The magnetic probes are placed behind the outer contour of the blanket and the divertor, 127 in total, and its direction is consistent with the local magnetic field direction of the standard configuration, as shown in Fig. 1(b).

In the real experimental environment, all diagnostics are affected by the measurement noise, and the noise should be modelled. The measuring noise comprises multiplicative and additive ones. The measurement noise of generic magnetic diagnostic i can be modelled through the following model:

$$y_{\mathrm{n}_i} = (1+n_{\mathrm{r}_i})y_i + n_{\mathrm{a}_i}, \tag{1}$$

where y_{n_i} describes the noisy measured value, the multiplicative and additive noises, denoted by n_{r_i} and n_{a_i}, are chosen as zero-mean Gaussian noises with standard deviations σ_{r_i} and σ_{a_i}, respectively.

The standard deviation of the measuring error due to noise depends on the selection of equilibrium, which indicated with l ($l = 1,2,\ldots,N$):

$$\sigma_i(l) = \sqrt{E[y_{\mathrm{n}_i}(l) - y_i(l)]^2} = \sqrt{\sigma_{\mathrm{r}_i}^2 y_i^2(l) + \sigma_{\mathrm{a}_i}^2}, \tag{2}$$

where l represents the selected equilibrium, E describes the mathematical expectation operator. $\sigma_i(l)$ has the following two bounds:

$$\sigma_i' \le \sigma_i(l) \le \sigma_i'', \tag{3}$$

where

$$\sigma_i' = \min_{l=1,2,\ldots,N} \sigma_i(l), \quad \sigma_i'' = \max_{l=1,2,\ldots,N} \sigma_i(l).$$

For CFETR, the measurement noise's maximum and minimum standard deviations for flux loops and magnetic probes are chosen as 9.72 mWb and 11 mT, and 2.16 mWb and 0.96 mT, respectively. To evaluate the design's efficiency, the random errors of normal distribution with a confidence level of 95% are added, where the relative error is 0.3%, and the absolute error is added according to the maximum standard deviation.

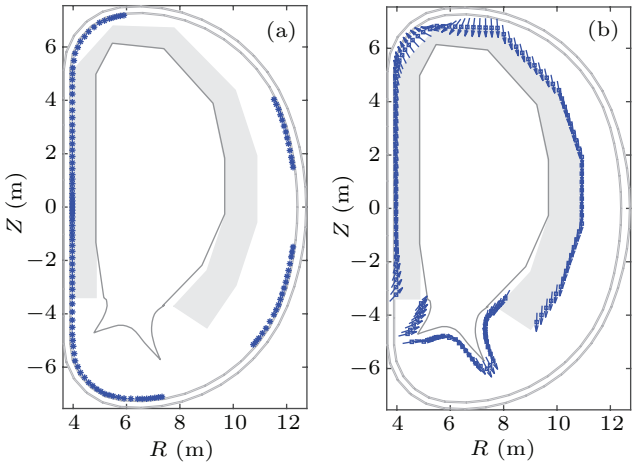


Fig. 1. Preliminary design of flux loops and magnetic probes on CFETR: (a) flux loops, (b) magnetic probes.

3. Optimizing the number of magnetic diagnostics based on TSVD

The TSVD approach was utilized to optimize magnetic diagnostics. This similar estimation is performed on ITER obtained satisfactory results[12] and verified in the EAST experiment.[13]

To optimize the magnetic diagnostics through the TSVD method, a large amount of equilibrium data is required at first. The Tokamak Simulation Code (TSC) can be used to simulate the time-dependent plasma performance in different phases of the discharge, including ramp-up, flat-top, and ramp-down.[19,20] CFETR has a variety of discharge parameters with different power levels, and in this paper, the 200-MW operating scenario in Table 1 of Ref. [2] is selected, in a flat-top slice ($t = 50$ s, $I_{\mathrm{p}} = 10$ MA, $\beta_{\mathrm{p}} = 0.081$, and $l_{\mathrm{i}} = 1.02$) for validation.

In showing the effect of plasma equilibrium reconstruction more intuitively, some locations are selected to determine the boundary errors. Three segments and one X point (presented in Fig. 2) are chosen for the computation. The boundary reconstruction error is described as a distance error on the segment, and the positive orientation is from the plasma core to the boundary. According to ITER's standards, the boundary reconstruction accuracy of seg 2 should be better than 2.5 cm, and the accuracy of other segments and X_{pt} should be better than 1 cm.

To verify the plasma equilibrium of TSC's simulation and the reconstruction quality of preliminary dense distribution, the above time slices were validated using EFIT code. Based on this time slice, add 100 sets of random errors that follow the

normal distribution. The plasma boundary error reconstructed by the EFIT code is shown in Fig. 3, with all position boundary errors less than 1 cm.

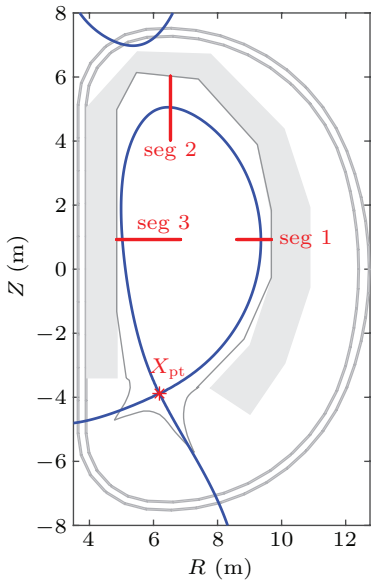


Fig. 2. The three CFETR control segments and the X point.

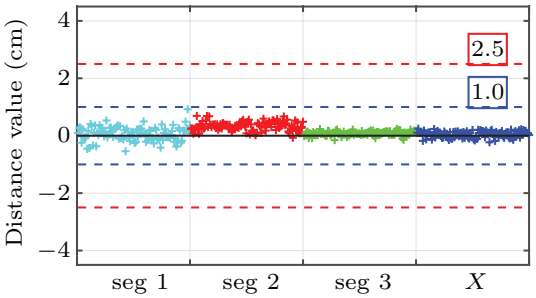


Fig. 3. Boundary errors of each control segment after adding the random error.

In the optimization of magnetic diagnostics, 10-MA scenarios are selected to establish a database. A total of 943 time slots were selected, including 431 ramp-up stages (31 are limiter configurations), 312 flat-top stages, and 200 ramp-down stages. The evolution of the plasma boundary in the ramp-up stage is shown in Fig. 4. The main parameters such as plasma current are shown in Table 1, plasma current ranges from 1 MA to 10 MA, consumes 140.55-Wb flux provided by PF coils to heat the plasma and ramp-up the plasma current, poloidal beta β_p ranges from 0.081 to 0.59, and internal inductance l_i ranges from 0.75 to 1.22.

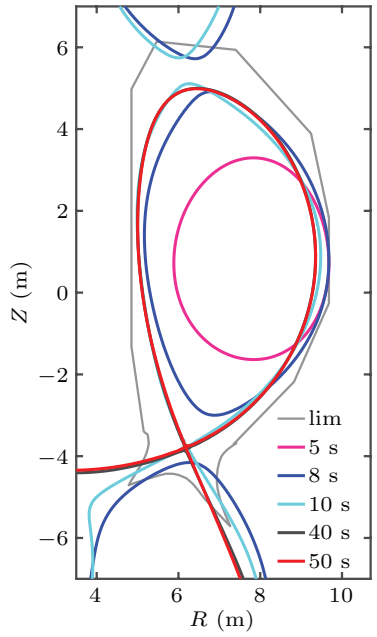


Fig. 4. Evolution of plasma boundary in the ramp-up stage.

Table 1. Main parameters.

Time (s)	5	8	10	20	40	50	60	80	100	120
I_p (MA)	1	1.6	2	4	8	10	10	10	10	10
Flux (Wb)	14.05	22.21	29.76	56.21	112.44	140.55	140.55	140.55	140.55	140.55
β_p	0.14	0.115	0.128	0.14	0.093	0.081	0.375	0.466	0.57	0.59
l_i	1.13	1.22	1.17	0.95	0.98	1.02	0.95	0.85	0.78	0.75

According to the above equilibrium, the measurement matrix is constructed for the flux loops and magnetic probes respectively:

$$F = \begin{bmatrix} f_1^{\mathrm{T}} \\ f_2^{\mathrm{T}} \\ \vdots \\ f_M^{\mathrm{T}} \end{bmatrix}, \tag{4}$$

where $F \in R^{M\times N}$, for flux loops and magnetic probes, $M = 117$, $N = 943$ and $M = 130$, $N = 943$ are chosen, respectively. The i-th row is the measurement of the i-th diagnostics in all the equilibria. Notably, for reliable results, $M \ll N$. The measurement matrix's SVD can be described as follows:

$$F = USV^{\mathrm{T}}. \tag{5}$$

Figure 5 presents the measurement matrix's singular values. Matrix F is full-rank with positive singular values. Although matrix F is a full-rank matrix with each singular value greater than zero, some singular values are much smaller than others which could be truncated, then the original matrix F could be transformed into a low-rank matrix F_k.

According to truncated SVD decomposing a matrix into its singular values and vectors and then selecting only the top k singular values and vectors, $k < \mathrm{rank}(F)$. Because a portion

of the three matrices were truncated, $U_k S_k V_k^{\mathrm{T}}$ is approximate to matrix F, which can be expressed as

$$F_k = U_k S_k V_k^{\mathrm{T}} \approx F. \tag{6}$$

If F_k can almost describe the initial matrix, a low-rank matrix exists that almost equals the initial matrix. In other words, using fewer diagnostics can provide almost identical information as using all diagnostics, the rank of the F_k is the number of the optimized diagnostics. The metric for verifying the approximate of the two is to meet the following inequality:

$$|\tilde{f}_i - f_i|_{\max} < \sigma_i', \tag{7}$$

where f_i indicates the i-th row in F, $\tilde{f}_i$ describes the i-th row in F_k, and $|\tilde{f}_i - f_i|_{\max}$ indicates the maximum absolute value of the error induced by reducing the measurement matrix's rank in all magnetic diagnostics σ_i' describes each diagnostic's minimum standard deviation. An appropriate truncation is obtained if the error induced by TSVD is smaller than the measuring noise.

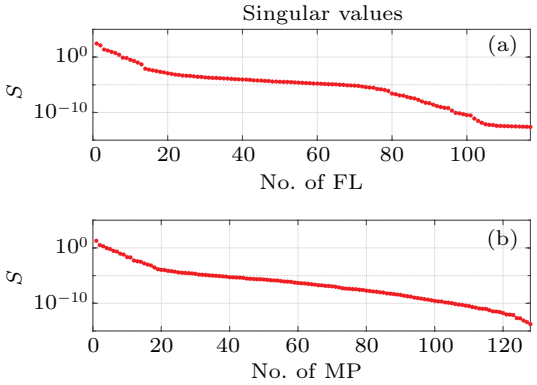


Fig. 5. The measurement matrix's singular values. FL: flux loop, MP: magnetic prob.

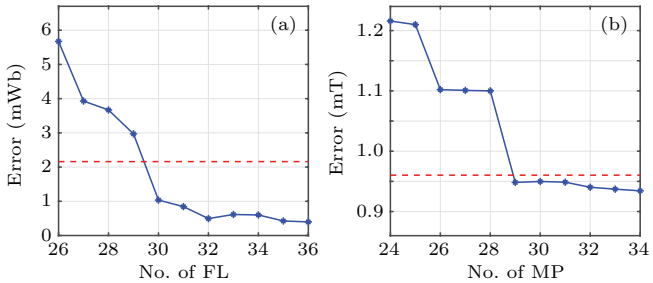


Fig. 6. The maximum error is introduced on the measurement matrix by rank reduction: (a) flux loops and (b) magnetic probes. The red dash line is the minimum uncertainty (flux loops: 2.16 mWb, magnetic probes: 0.96 mT).

Equation (7) indicates that the minimum value σ_i' is of greater concern. The CFETR's chosen standard deviation was presented in Section 2. Firstly, gradually reducing the rank of the matrix, that is, gradually reducing the number of magnetic diagnoses until equation (7) is violated. Figure 6 shows the maximum error introduced by the rank reduction of the flux loop (FL) and magnetic probe (MP) measurement matrix, requirements (error < minimum uncertainty mentioned in Section 2), which indicates that the number of flux loops and magnetic probes can be reduced to 30 and 29. Secondly, the maximum errors for each row, resulting from the comparison of matrix F to matrix F_k, are obtained and sorted. This maximum error is introduced by TSVD on each magnetic diagnostic signal. The larger error indicates that affection by rank reduction on the magnetic diagnostic signal is non-negligible and the magnetic diagnostic should be retained. Figure 7 describes each magnetic diagnostic's error sequence. Based on the above two steps, the optimized layout of magnetic diagnoses can be obtained (shown in Fig. 8).

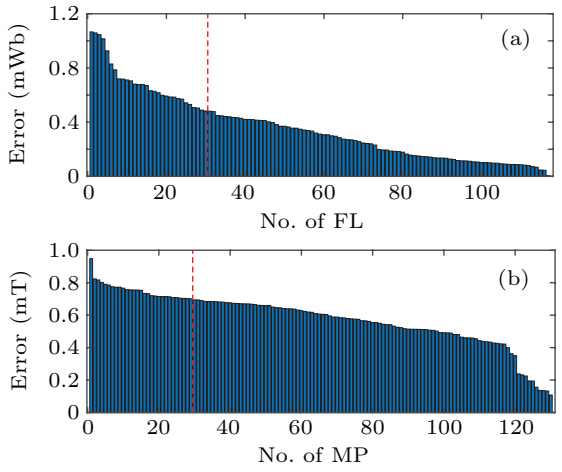


Fig. 7. Each magnetic diagnostic's maximum error after reducing the measurement matrix's rank: (a) flux loops and (b) magnetic probes.

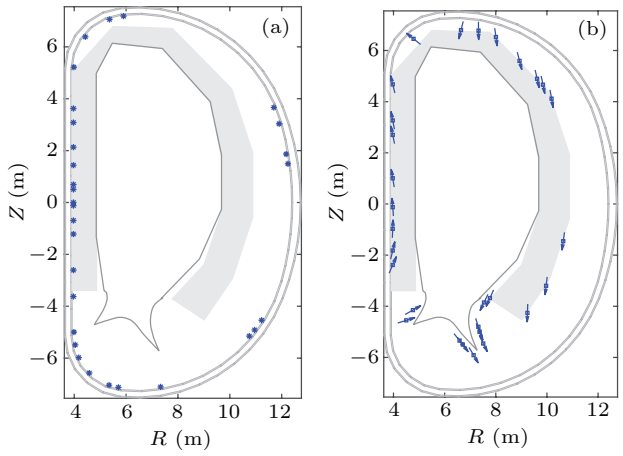


Fig. 8. The CFETR-reduced magnetic diagnostics: (a) flux loops and (b) magnetic probes.

4. Reliability verification by a plasma reconstruction code

To verify the results attained in Section 3, the reconstruction of the equilibrium of the plasma using 30 flux loops and 29 magnetic probes was compared with that calculated using fixed boundaries by the EFIT code.

4.1. Verifying the optimization results using 10-MA scenarios

Firstly, five time slices are selected in the flat-top stages ($t = 50$ s, 60 s, 80 s, 100 s, 120 s, and $I_p = 10$ MA), and 100 sets of random errors are added. The reconstructed plasma equilibrium is compared by the EFIT code with the target equilibrium. As shown in Fig. 9, for 496 out of 500 equilibria, the plasma current estimation error is below 1%, and the β_p and l_i estimation error is within $\pm(0.05 + 5\%)$, where 0.05 is the absolute error, and 5% is the relative error. The boundary calculation results are shown in Fig. 10. It can be noted that, in the flat-top cases, the boundary estimation error is always less than 2.5 cm in seg 2, and only 3 equilibria exceed 1 cm in other positions. However, the maximum error is below 1.2 cm in all the mentioned cases. Accordingly, for the flat-top stage which is the most important for CFETR, these magnetic diagnostics can effectively reconstruct plasma equilibrium.

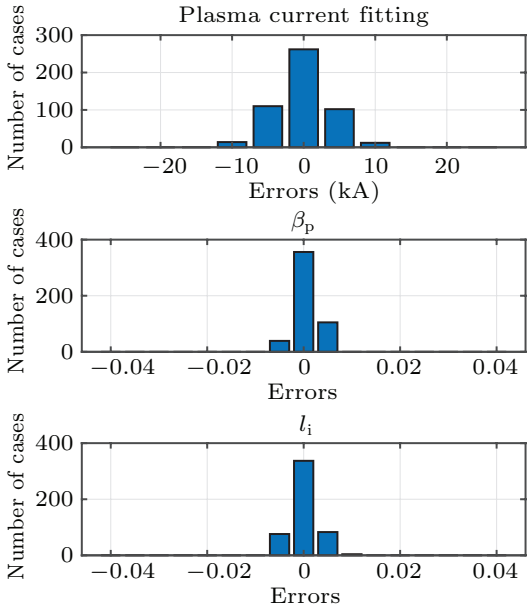


Fig. 9. Macroscopic parameters calculation quality.

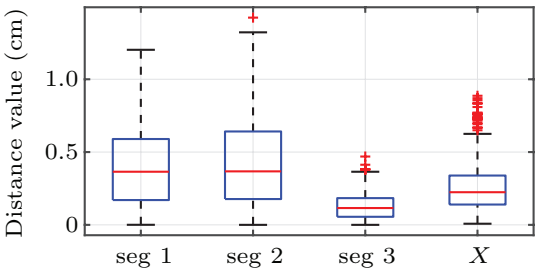


Fig. 10. Plasma boundary absolute errors reconstruction (red line describes the median, blue box indicates the first and third quartiles and red crosses describe the outliers).

4.2. Verifying the optimization results using 14-MA scenarios

Apart from the 10-MA scenarios, CFETR has higher parameter designs.[2] The case of selecting a plasma current of 14 MA further verifies the design of the magnetic diagnostics. Similarly, 100 sets of random errors were added to the magnetic measurement data, their macroscopic parameters calculation quality is shown in Fig. 11, and their boundary fitting errors are shown in Fig. 12, all of which meet the accuracy standards.

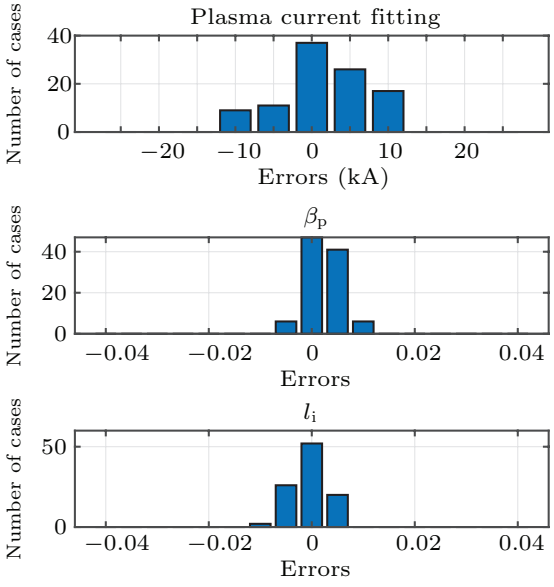


Fig. 11. Macroscopic parameters calculation quality ($I_p = 14$ MA).

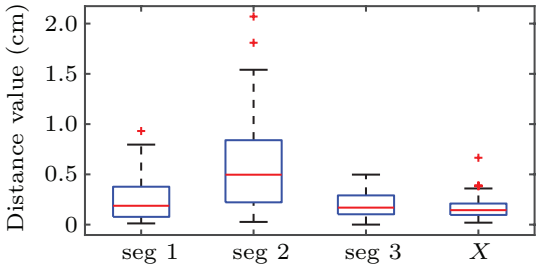


Fig. 12. Boundary errors of each control segment ($I_p = 14$ MA).

4.3. Verifying the optimization results with the ramp-up phase

Within the ramp-up stage, when the plasma current is higher than 4 MA, the reconstruction results meet the accuracy requirements, their macroscopic parameters calculation quality is shown in Fig. 13, and the boundary error is presented in Fig. 14. When the plasma current is lower than 4 MA, the reconstructed boundary error on seg 2 exceeds 2.5 cm, while the error on other segments is still below 1 cm as shown in Fig. 15.

In the ramp-up phase, because of the small plasma current and eddy currents, the magnetic diagnostic signals have relatively smaller contributions from plasma. It is well known that this situation is the main cause of the low quality of the reconstruction. Moreover, accurate results cannot be obtained even when employing all magnetic diagnostics as shown in Fig. 15. At this stage, the accuracy requirements of equilibrium parameters for plasma control are not very high. The

optimized magnetic diagnostics can meet the CFETR plasma operation and control requirements.

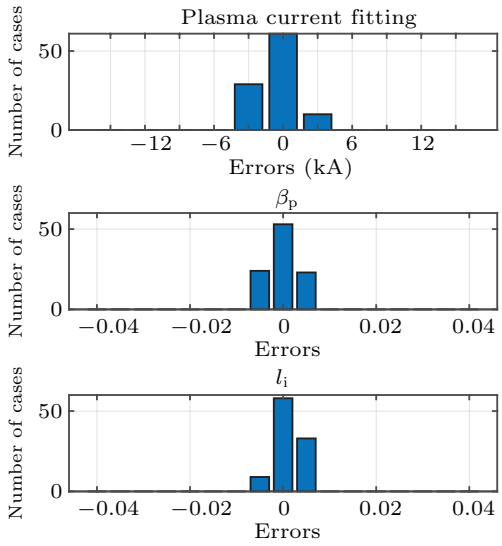


Fig. 13. Macroscopic parameters calculation quality ($I_p = 4$ MA).

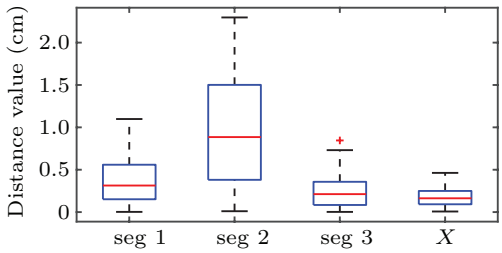


Fig. 14. Boundary errors of each control segment ($I_p = 4$ MA).

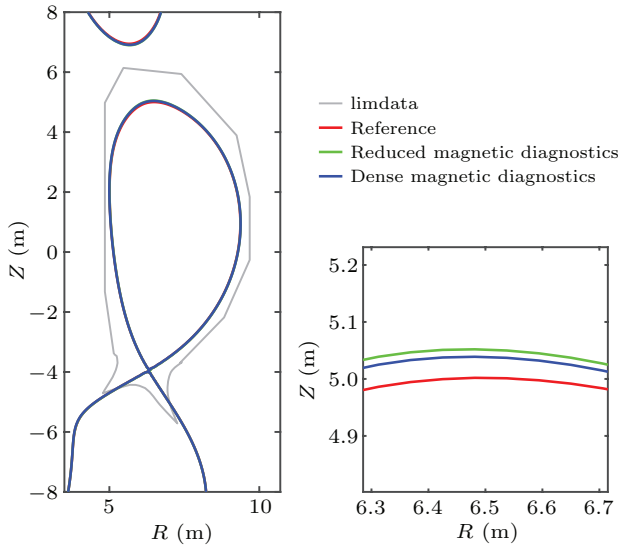


Fig. 15. The boundary reconstruction result of CFETR 3-MA scenarios (The distance between the reduced and dense magnetic diagnostics reconstruction boundaries and the reference boundary are 4.89 cm and 3.60 cm, respectively, on seg 2).

5. Discussion and conclusion

This paper designs and optimizes the magnetic diagnostics layout for CFETR plasma equilibrium reconstruction. With the synthetic magnetic measurement data, EFIT code is utilized to obtain plasma equilibrium which is consistent with the TSC code simulation. On this basis, add the random error, and simulate the real experimental environment to verify the effectiveness of the design. The TSVD method is used to optimize the number and location of magnetic diagnostics, reducing them to 30 flux loops and 29 magnetic probes, and reconstructing the plasma equilibrium that meets the accuracy requirements, further verifying the redundancy reliability of the magnetic diagnostics layout design. This work provides a design approach for the magnetic diagnostics layout system required for the equilibrium control of CFETR. The developed design and optimization method can effectively support designing magnetic diagnostics systems in future magnetic confinement fusion devices.

Data availability statement

The data generated and/or analyzed during the current study are not publicly available for legal/ethical reasons but are available from the corresponding author on reasonable request.

Acknowledgements

The authors are grateful to the EAST team for providing the experimental data. Project supported by the National MCF Energy Research and Development Program of China (Grant Nos. 2022YFE03010002, 2018YFE0302100, and 2018YFE0301105) and the National Natural Science Foundation of China (Grant Nos. 11875291, 11805236, 11905256, and 12075285).

References

[1] Song Y T, Wu S T, Li J G, Wan B N, Wan Y X, Fu P, Ye M Y, Zheng J X, Lu K, Gao X G, Liu S M, Liu X F, Lei M Z, Peng X B and Chen Y 2014 *IEEE Trans. Plasma Sci.* **42** 503
[2] Zhuang G, Li G Q, Li J, Wan Y X, Liu Y, Wang X L, Song Y T, Chan V, Yang Q W, Wan B N, Duan X R, Fu P and Xiao B J 2019 *Nucl. Fusion* **59** 112010
[3] Lao L L, John H St, Stambaugh R D, Kellman A G and Pfeiffer W 1985 *Nucl. Fusion* **25** 1611
[4] Lao L L, John H E St, Peng Q, Ferron J R, Strait E J, Taylor T S, Meyer W H, Zhang C and You K I 2005 *Fusion Sci. Technol.* **48** 968
[5] Strait E J, Fredrickson E D, Moret J M and Takechi M 2008 *Fusion Sci. Technol.* **53** 304
[6] Peruzzo S, Albanese R, Artaserse G, Coccorese V, Gerasimov S, Lam N, Maviglia F, Pearson I, Prior P, Quercia A, Zabeo L and JET-EFDA Contributors 2009 *Fusion Eng. Des.* **84** 1495
[7] Kim H S, Bak J G and Hahn S H 2017 *Fusion Eng. Des.* **123** 641
[8] Strait E J 2006 *Rev. Sci. Instrum.* **77** 023502
[9] Shen B, Luo J R, Wan B N and Wang H Z 2003 *Plasma Sci. Technol.* **5** 1785
[10] Testa D, Toussaint M, Chavan R, Guterl J, Lister J B, Moret J M, Perez A, Sanchez F, Schaller B, Tonetti G, Encheva A, Vayakis G, Walker C, Fournier Y, Maeder T, Le-Luyer A, Moreau P, Chitarin G, Alessi E, Delogu R S, Gallo A, Marconato N, Peruzzo S, Preindl M, Carfantan H, Hodgson E, Romero J, Vila R, Brichard B and Vermeeren L 2010 *IEEE Trans. Plasma Sci.* **38** 284

[11] Biel W, Albanese R, Ambrosino R, Ariola M, Berkel M V, Bolshakova I, Brunner K J, Cavazzana R, Cecconello M, Conroy S, Dinklage A, Duran I, Dux R, Eade T, Entler S, Ericsson G, Fable E, Farina D, Figini L, Finotti C, Franke T, Giacomelli L, Giannone L, Gonzalez W, Hjalmarsson A, Hron M, Janky F, Kallenbach A, Kogoj J, König R, Kudlacek O, Luis R, Malaquias A, Marchuk O, Marchiori G, Mattei M, Maviglia F, Masi D G, Mazon D, Meister H, Meyer K, Micheletti D, Nowak S, Piron C, Pironti A, Rispoli N, Rohde V, Sergienko G, Shawish E S, Siccinio M, Silva A, Silva F, Sozzi C, Tardocchi M, Tokar M, Treutterer W and Zohm H 2019 *Fusion Eng. Des.* **146** 465

[12] Pironti A, Albanese R, Ambrosino G and Ariola M 52*nd IEEE Conference on Decision and Control (CDC)*, December 10–13, 2013, Florence, Italy, pp. 4200–4205

[13] Yu Q Z, Huang Y, Luo Z P, Wang Y H, Liu Z J, Rui W Y, Wu K, Chen D L, Shen B, Xiao B J and Li J G 2023 *Plasma Phys. Control. Fusion* **65** 055013

[14] Formisano A, Martone R and Trevisan F 2001 *COMPEL — The International Journal for Computation and Mathematics in Electrical and Electronic Engineering* **20** 523

[15] Tommasi D G, Neto A C, Pironti A and Sterle C 2015 *IEEE Conference on Control and Applications (CCA)*, September 21–23, 2015, Sydney, Australia, pp. 1296–1302

[16] Chlechowitz E, Talmadge J N, Hanson J D, Anderson F S B and Anderson D T 2015 *Nucl. Fusion* **55** 113012

[17] King J D, Strait E J, Boivin R L, Taussig D, Watkins M G, Hanson J M, Logan N C, Paz-Soldan C, Pace D C, Shiraki D, Lanctot M J, Haye L R J, Lao L L, Battaglia D J, Sontag A C, Haskey S R and Bak J G 2014 *Rev. Sci. Instrum.* **85** 083503

[18] Neilson G H, Basile A, Cohen A, Cometa F, Looz D M A, Fair R, Gattuso A, Jariwala A, Muscatello C, Pablant N, Paraiso G, Shirey S, Smith M, Zolfaghari A and Team U I D 2022 *IEEE Trans. Plasma Sci.* **50** 4144

[19] Liu L, Wang M, Mao S F, Guo Y, Luo Z P, Jian X, Liu X F, Zu C, Chan V and Ye M Y 2017 *Fusion Eng. Des.* **123** 137

[20] Liu C Y, Wu B, Qian J P, Li G, Hou Y, Wei W, Chen M X, Lei M Z and Guo Y 2020 *Chin. Phys. B* **29** 025202